A Growth Mechanism for Topographic Internal Waves Generated by an Oscillatory Flow

TOMOHIRO NAKAMURA AND TOSHIYUKI AWAJI

Department of Geophysics, Graduate School of Science, Kyoto University, Kyoto, Japan

8 December 1999 and 26 February 2001

ABSTRACT

On the basis of ray tracing of individual waves generated at various phases of the tidal flow, an amplification mechanism is presented for a new class of topographically generated internal waves identified by Nakamura et al., which develop across a broad latitude range and can exist even above the critical latitude where the tidal frequency equals the inertial frequency. The results show that unsteady lee waves are always amplified when the maximum frequency is much smaller than the buoyancy frequency because their phase speeds (amplitudes) are equal (proportional) to the tidal flow speed at their time of generation. Fast mixed tidal–lee waves are also effectively amplified, when the rotation effect is significant. Accordingly, amplification of unsteady lee and fast mixed tidal–lee waves can occur even if the requirements of previous theories (e.g., the critical slope and critical Froude number conditions) are not satisfied. Since the result here covers the generation and amplification processes of topographic internal waves across a broader parameter range than earlier theories, it should contribute to a better understanding of boundary mixing processes, especially in high-latitude regions.

1. Introduction

The generation of large-amplitude internal waves by tidal currents is a subject of increasing research interest because recent studies reveal that vertical mixing effects caused by the breaking of tidally generated internal waves at open-ocean boundaries—the so-called boundary mixing problem (e.g., Lukas et al. 1996)—can significantly affect large-scale processes in the open ocean. The interactions between waters of the Okhotsk Sea and those of the North Pacific Ocean via the Kuril Straits, for example, can be considered to be a typical boundary mixing problem. Several studies (Talley 1991; Kono and Kawasaki 1997) show that sill-related vertical mixing in the Kuril Straits is an important factor in the production of the North Pacific Intermediate Water and suggest that interactions between swift tidal currents and sill topography at the Kurils is a likely cause for the intense vertical mixing. In order to clarify this mechanism, Nakamura et al. (2000, hereafter NA) recently performed numerical simulations of tidally generated internal waves over a representative sill in the Kuril Straits (~47°N; Fig. 1), using a two-dimensional nonhydrostatic f-plane model to distinguish the physics of the waves generated for both subinertial K_1 and superinertial M_2 cases. Their results showed a number of interesting phenomena that are difficult to explain on the basis of present internal wave theories.

The formation of large-amplitude internal waves by a tidal flow is normally considered to involve the following three stages. First, tide–topography interactions generate internal waves at the tidal frequency (internal tides), and the waves are considerably amplified if the slope of their characteristics is equal to that of the topography (the ''critical slope'' condition: Wunsch 1969; Baines 1982; Craig 1987; Sherwin 1988; Sherwin and Taylor 1990; reviews by Wunsch 1975; Huthnance 1989). The second stage is the amplification of internal tides at their generation regions. This process is thought to be most important and was investigated by Hibiya (1986, hereafter HI), using the modal wave approximation. He showed that when a barotropic tidal flow is critical [i.e., the internal Froude number, defined as the ratio of the barotropic flow speed $U(t)$ to phase velocity of the nth mode c_n, $F_n = U(t)/c_n$, is unity], internal tides propagating upstream are trapped within the generation region and amplified to form large-amplitude internal waves. When the tidal flow falls below the critical Froude number, the waves begin to propagate upstream away from the generation region. The third stage represents the nonlinear evolution of the large-amplitude internal waves as they propagate away from the gen-

Corresponding author address: Dr. Tomohiro Nakamura, Dept. of Geophysics, Graduate School of Science, Kyoto University, Kyoto 606-8502, Japan.
E-mail: nakamura@kugi.kyoto-u.ac.jp

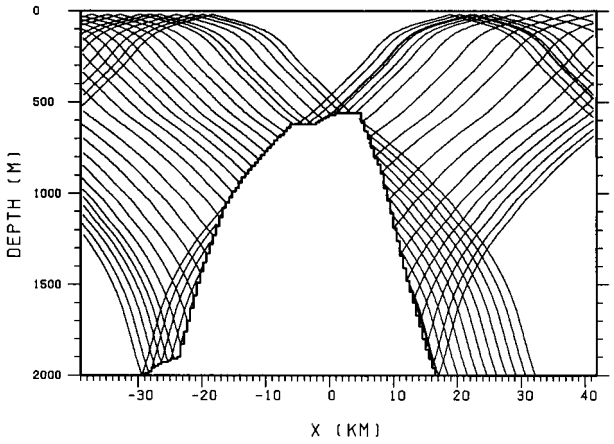

FIG. 1. The characteristics of the M_2 internal tides in the model of NA. The slope of the right-hand side of the sill is supercritical.

eration region. Investigations using the KdV equation or its alternatives showed that when the wave amplitude is sufficiently large, internal tides grow and disintegrate into large-amplitude solitary wave trains (e.g., Lee and Beardsley 1974; Mazé 1987; Willmott and Edwards 1987; Smyth and Holloway 1988; Gerkema and Zimmerman 1995). Generally, this process follows the second stage, after the amplified waves have propagated a certain distance from the generation region (Liu et al. 1985).

In the superinertial M_2 case of NA, short internal waves generated around the sill break were trapped and amplified within the generation region. As shown in Fig. 1, the right-hand slope in such a situation was significantly steeper than that of the characteristics of the M_2 internal tides, given by $[(\sigma_f^2 - f^2)/(N^2 - \sigma_f^2)]^{1/2}$ where N, f, and σ_f are the buoyancy frequency, the Coriolis parameter, and the tidal frequency, respectively. This blocks leftward propagation of the internal tides generated on the right-hand slope. Thus, the growth of the short wave is not consistent with the critical slope theory. Assuming the conventional modal wave theory near the sill top for convenience, we estimated the contribution rates and Froude numbers for the lowest seven modes at the right-hand break (see appendix A). Table 1 shows that the major vertical modes were the lowest three modes, but the maximum values of F_1, F_2, and F_3 were 0.33, 0.51, and 0.87, respectively. This suggests that the wave trapping and amplification in the M_2 case of NA is out of the range of the HI model.

Observations by Kuroda and Mitsudera (1995) captured similar phenomena in the shelfbreak region of the East China Sea, in which the first mode wave was trapped and amplified, eventually leading to a hydraulic-like jump in the isopycnal surfaces when $F_1 = 0.71$. They interpreted the wave trapping with a steady hydraulic control theory, taking into consideration the effect of the decrease in wave speed due to advection at large amplitudes (Grimshaw and Smyth 1986). However, their theoretical model does not effectively explain the wave trapping in the NA case in which the Froude number is considerably less than unity (for example, $F_1 \sim 0.3$). In addition, the isopycnal displacement of the short wave in NA is about 20 m, which in a depth of 550 m is too small to cause the wave speed decreases reported in Kuroda and Mitsudera (1995).

The other important result presented in NA was that the K_1 flow over the sill generates large-amplitude internal waves that propagate away from the sill, even though the K_1 tide is subinertial at the Kuril Straits (see Figs. 6 and 7 of NA). This posed the question as to how these waves come about since subinertial internal tides are topographically trapped waves.

From theoretical considerations, NA revealed the nature of internal waves generated by a tidal flow using the new nondimensional parameter kU_0/σ_f, where k is the horizontal wavenumber and U_0 is the tidal flow amplitude. As is summarized in Table 1, in the case of $kU_0/\sigma_f \gg 1$, the generated waves are characterized as unsteady lee waves with intrinsic frequencies of $-kU(t)$, and amplitudes depending on $U(t)h_x$ (h_x is the slope of the bottom topography). Thus, all wave properties except for $|k|$ are defined at the generation time. In contrast, when $kU_0/\sigma_f \ll 1$, internal tides are generated, whose frequency is almost constant and is identical to the tidal frequency in the limit $kU_0/\sigma_f \to 0$. Internal

TABLE 1. The modal decomposition result of vertical velocity for the M_2 case after 1/8, 1/4, 3/8, and 1/2 period. In order to focus on the short internal wave over the right-hand sill break, velocity data at the break are analyzed here. C.T.: contribution rate, R.M.: relative magnitude, and Fr: Froude number.

	1/8 tidal period			2/8 tidal period			3/8 tidal period			4/8 tidal period		
Mode no.	C.R. (%)	R.M. (10^{-1})	Fr	C.R. (%)	R.M. (10^{-1})	Fr	C.R. (%)	R.M. (10^{-1})	Fr	C.R. (%)	R.M. (10^{-1})	Fr
1	48.76	−1.55	0.23	21.72	−1.69	0.33	8.33	0.75	0.23	21.88	1.38	0.00
2	40.94	2.01	0.37	54.85	3.81	0.51	29.73	2.01	0.37	69.76	−3.50	0.00
3	6.27	−0.71	0.61	12.48	−1.63	0.87	29.92	−1.81	0.61	0.01	0.03	0.00
4	2.84	0.52	0.80	7.00	1.33	1.13	21.25	1.65	0.80	4.51	0.87	0.00
5	1.15	−0.29	0.99	2.42	−0.69	1.40	6.12	−0.78	0.99	3.33	−0.66	0.00
6	0.66	0.25	1.19	1.33	0.58	1.69	2.63	0.58	1.19	1.12	0.43	0.00
7	0.47	−0.20	1.39	0.81	−0.43	1.97	1.28	−0.38	1.39	0.33	−0.22	0.00
sum	101.08			100.60			99.26			100.92		

tides propagate in both directions, as previous studies indicated. In the intermediate range of $kU_0/\sigma_f \sim 1$, waves with properties intermediate between those of lee waves and internal tides (and are named ''mixed tidal-lee waves'' by NA, hereafter MTL waves) are generated, with intrinsic frequencies of $-kU(t) \pm \sigma_f$. Thus, the MTL wave splits into two components propagating with different phase velocities.

The nature of the unsteady lee and MTL waves not only allows us to understand the generation mechanism of free-propagating internal waves by a subinertial flow (as described above) but can also account for their trapping at sills, which leads to significant wave amplification. The intrinsic horizontal phase speeds of the internal tides ($\pm\sigma_f/k$) are constant. However, those of the unsteady lee waves and MTL waves [$-U(t)$ and $-U(t) \pm \sigma_f/k$, respectively] vary with the phase of the tidal flow at their generation time. This affects the way in which the individual wave components of these waves superpose. For example, the phase speeds of unsteady lee waves are equal to the basic flow speed at their generation time for all current speeds (as long as $f < |kU \pm \sigma_f| < N$), suggesting a tendency to be trapped and superposed in the generation region. A similar propagation feature was found in numerical experiments on an oscillatory flow over the shelf slope with small length-scale ripples by Thorpe (1996), who suggested that the propagation time of internal motions from the generation region to the shelf break depends on a parameter $kU(t)/\sigma_f$, though his theory (Thorpe 1992, 1996) assumed a steady flow condition. However, such effects have not been investigated in any depth in previous theories, though it is clear that the dynamics of lee waves, and in particular their transient propagation processes, should be incorporated into any representative account of wave growth.

Lott and Teitelbaum (1993a,b) studied atmospheric lee waves using a similar approach to NA. Though they described many interesting features of unsteady lee waves, the effect of the time variation of forcing on wave excitation was neglected and, hence, the short wave growth in an oscillatory flow regime lies outside the scope of their work. Also, Bell (1975) considered a situation similar to NA, and Bannon and Zehnder (1985) added a steady flow component to Bell's model. However, since internal waves in these studies are treated as an infinite series of modes in the temporal domain, the characteristic features of unsteady lee waves and MTL waves were not clearly described.

In this study, we investigate the growth mechanism of topographic internal waves generated by an oscillatory flow, focusing specifically on the unsteady lee waves and MTL waves. In doing so, we use a ray tracing approach for individual wave growth because a modal decomposition is not strictly valid for the finite-amplitude sill case of NA due to complicated energy conversion between different modes. In addition, application of the modal decomposition is less suitable for transient waves (see Fig. 7 of NA) that are generated around the sill top and have not been reflected at the surface (a variety of vertical modes are required for identification and characterization of the aspects of wave growth, Rattray et al. 1969). This is so, in a sense, for unsteady lee and MTL waves since their frequencies vary with the phase of a tidal flow. To gain an understanding of the wave growth mechanism, ray tracing might therefore be a simpler and more relevant approach than a modal expansion.

The outline of this paper is as follows. In section 2 a new amplification mechanism for tidally generated internal waves is proposed, and in section 3 ray tracing of individual waves is performed to demonstrate the effectiveness of our amplification mechanism. The conclusions are summarized and discussed in section 4.

2. The growth mechanism of topographic internal waves

In this section, we examine the growth mechanism of a compound wave formed by the superposition of individual waves, taking into consideration the transient propagation process of individual wave components.

a. Wave growth in each wave regime

First, we investigate the propagation and associated superposition of wave components in the horizontal direction. To highlight the difference due to wave types, we begin with the convenient case in which the group speed $|c_g|$ is nearly equal to the phase speed $|c_p|$ in both horizontal and vertical directions:

$$|c_g| = |c_p|\left(1 - \frac{\sigma_i^2}{N^2}\right)\left(\frac{1 - f^2/\sigma_i^2}{1 - f^2/N^2}\right) \simeq |c_p|\left(1 - \frac{\sigma_i^2}{N^2}\right)\left(1 - \frac{f^2}{\sigma_i^2}\right) \simeq |c_p|. \quad (1)$$

The above case corresponds to assuming individual waves with frequencies of $f \ll \sigma_i \ll N$ (other cases will be discussed later). To define the fundamental mechanism of wave growth clearly, the following simplifications are made, which can be easily relaxed: The basic flow and stratification are uniform and, as modal waves still have not been formed, the wavenumbers can be determined from the horizontal scale of forcing, the intrinsic frequency σ_i, and the dispersion relation. In this situation, forcing at $t = t_0$ generates two individual waves with horizontal phase velocities of

$$c_{px}^{\pm}(t_0) = U_0\left(-\frac{U(t_0)}{U_0} \pm \frac{\sigma_f}{kU_0}\right), \quad (2)$$

where the upper (lower) signs correspond to each other. Thus, the growth of compound waves formed by these wave components depends on the parameter kU_0/σ_f, as

this determines the shapes of ray paths and hence their superposition.

The positions, $x^{\pm}(t)$, of the two wave components mentioned above are

$$x^{\pm}(t) = c_{gx}^{\pm}(t_0)(t - t_0) + \int_{t_0}^{t} U(\tau)\, d\tau, \qquad (3)$$

where the generation point is set to be $x = 0$. We consider a basic flow of $U(t) = U_0 \sin(\sigma_f t)$, which begins to accelerate rightward from $U = 0$ at $t = 0$, as in NA. Figure 2 shows the loci of individual wave components during one tidal cycle for various kU_0/σ_f values, in which the tidal excursion U_0/σ_f is kept constant. Wave components of phase velocity $c_{px}^{-}(c_{px}^{+})$ are shown in Fig. 2-column 1 (Fig. 2, column 2), and their amplitudes are represented by line thickness.

1) Unsteady lee wave regime

When $kU_0/\sigma_f \gg 1$, both horizontal phase velocities $c_{px}^{\pm}(t_0)$ are almost equal and in the opposite direction to the basic flow velocity at their generation time [i.e., $-U(t_0)$]. Accordingly, Figs. 2(1a) and 2(1b) are almost identical and have the following features: Wave components generated during the acceleration stage of rightward flow ($0 \sim 1/4$ period) move downstream from the generation point until the basic flow decelerates to speeds that match those at their generation time. This is because the phase speed of an individual wave component remains equal to the flow speed at the generation time, while the basic flow continues to accelerate and so becomes faster than the speed of the wave component. On the other hand, wave components generated during deceleration of the rightward flow ($1/4 \sim 1/2$ period) move upstream relative to the ground and accelerate since the basic flow slows down after their generation. After the flow turns to the left, all of these wave components move leftward since the direction of the basic flow becomes the same as that of the phase velocities of wave components generated during the rightward flow. The propagation of wave components generated in the latter half period ($1/2 \sim 1$ period) is the same as in the former half period but with the directions reversed.

The small time variation in flow speed around the time of maximum flow results in the formation of a distinct wave front. Now a condition persists under which the phase speeds of the individual wave components are almost equal to the basic flow speed. Accordingly, individual waves generated around this time are effectively trapped so that they superpose within the generation region. In addition, because the amplitudes are also proportional to the basic flow speed, these wave components have the largest amplitudes and hence the compound wave shows an apparent amplitude dispersion. Thus, individual waves generated around the time of maximum flow form a leading wave front that propagates with maximum phase speed and little dispersion in the upstream direction at the generation time and exports most of the wave energy generated in the half period. The other individual waves form a highly dispersive tail in which waves of low amplitude gradually disappear. Similar growth and propagation processes for short internal waves generated on the downstream side of a sill have been reported in observations (Farmer and Smith 1980).

In the K_1 case of NA, the growth process to the large-amplitude wave at the right-hand break can be understood by the above mechanism because here kU_0/σ_f is 5.4, indicating that this wave is roughly in the unsteady lee wave regime. This can be also interpreted in terms of a Froude number for individual waves, F_i, defined as the ratio of the basic flow speed $U(t)$ to the phase speed of each wave component. The F_i values are almost unity for individual unsteady lee waves when they are generated. As the basic flow accelerates (decelerates) and becomes supercritical (subcritical) where $F_i > 1$ (<1) after generation, the individual waves move downstream (upstream) relative to the seabed. At maximum flow speed, the condition $F_i \simeq 1$ is still maintained, and individual wave components generated at this time are trapped and superposed on each other at the generation point.

Although the application of modal wave theory to a transient wave field might not be suitable, the above description becomes qualitatively similar to the interpretation by conventional modal wave theories (e.g., HI), if the definition of the Froude number is extended to individual wave components (F_i). This enables us to easily understand the trapping process of tidally generated transient waves at sills. It should be noted, however, that transient wave phase speeds are equal to the basic flow speeds at their generation time regardless of the phase speeds of modal waves.

2) Internal tide regime

Because the horizontal phase velocities of wave components characterized as internal tides are always almost equal to $\pm\sigma_f/k$, when $kU_0/\sigma_f \ll 1$, the maximum value of the Froude number for internal tides F_i ($=kU_0/\sigma_f$)

→

FIG. 2. The loci of individual wave components in x–t space during one tidal cycle, when the parameter kU_0/σ_f is 10 (a), 2 (b), 1 (c), 0.5 (d), and 0.1 (e). Those of phase velocity c_{px}^{+} and c_{px}^{-} are shown in the left (1) and right (2) columns. Waves are generated at $x = 0$, the basic flow is directed rightward during $0 \leq$ period < 0.5 and leftward during $0.5 \leq$ period < 1, and the amplitudes of individual waves are represented by line thickness (for the case of symmetric forcing). The horizontal scale is dedimensionalized using the tidal excursion U_0/σ_f.

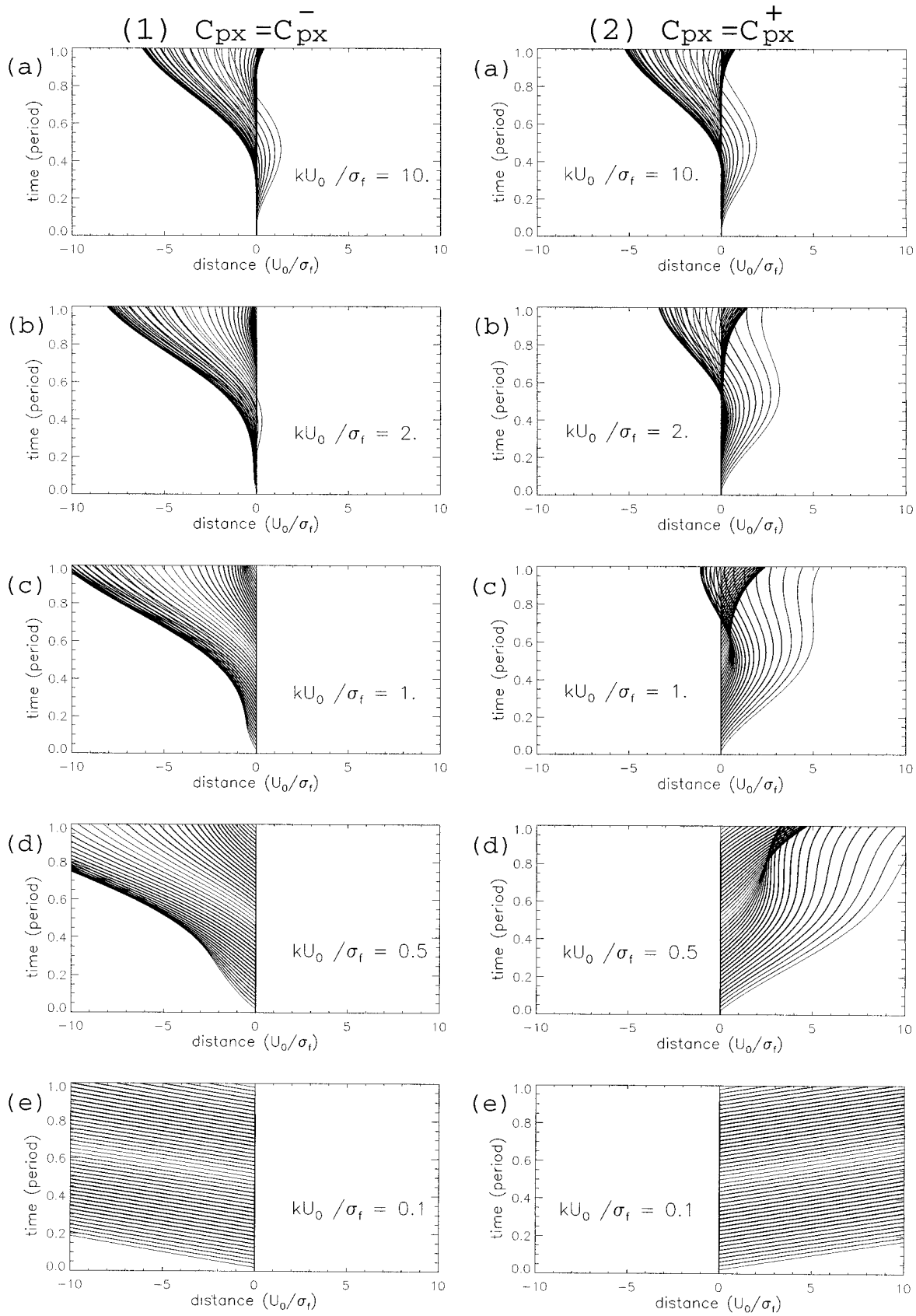
(1) $C_{px} = C_{px}^{-}$
(2) $C_{px} = C_{px}^{+}$
(a)
(b)
(c)
(d)
(e)
kU_0/σ_f = 10.
kU_0/σ_f = 2.
kU_0/σ_f = 1.
kU_0/σ_f = 0.5
kU_0/σ_f = 0.1
time (period)
distance (U_0/σ_f)

TABLE 2. Properties of tidally generated internal waves.

Regime	$\frac{kU_0}{\sigma_f} \gg 1$	$\frac{kU_0}{\sigma_f} \sim 1$	$\frac{kU_0}{\sigma_f} \ll 1$
Wave type	Unsteady lee waves	Mixed tidal–lee waves	Internal tides
Intrinsic frequency	$-kU(t)$	$-kU(t) \pm \sigma_f$	$\pm\sigma_f$
Relative phase velocity	$-U(t)$	$-U(t) \pm \sigma_f/k$	$\pm\sigma_f/k$

is much less than unity. Hence the effect of advection, which slightly slows down (speeds up) wave components propagating upstream (downstream), is too small to enable these components to superpose (Fig. 2e), and thus wave amplification never occurs. Therefore, large-amplitude waves are not formed except in the vicinity of the critical slope, as is indicated by previous studies.

3) MIXED TIDAL–LEE WAVE REGIME

When $kU_0/\sigma_f \sim 1$, the propagation of wave components with phase velocities of c_{px}^+ and c_{px}^- are quite different, making their loci asymmetric. Since the magnitudes of lee-wave $[-U(t)]$ and internal tide $(\pm\sigma_f/k)$ constituents are comparable in this range, the difference between horizontal phase velocities c_{px}^+ and c_{px}^- is significant, as with internal tides, while these phase velocities vary in time and the advection effect is significant, as with unsteady lee waves. For this reason, we separate MTL wave components on the basis of whether the phase velocity of their internal-tide constituent is in the same direction as the lee wave constituent, that is,

$$c_{px} = c_{px}^f = -U + \mathrm{sgn}(-U)\frac{\sigma_f}{k}, \tag{4}$$

or in the opposite direction, that is,

$$c_{px} = c_{px}^s = -U + \mathrm{sgn}(+U)\frac{\sigma_f}{k}. \tag{5}$$

We name the waves with phase velocities c_{px}^f and c_{px}^s ''fast'' and ''slow'' MTL waves, respectively. As is apparent from the definition, fast MTL waves are faster than both lee-wave and internal-tide constituents, whereas slow MTL waves propagating upstream (downstream) are slower than unsteady lee waves (internal tides).

In Fig. 2, the components of fast (slow) MTL waves generated in the former half period of rightward flow correspond to those with phase speeds c_{px}^- (c_{px}^+), and those in the latter half period to components with c_{px}^+ (c_{px}^-). The advection effect together with the significant differences in phase velocity between individual MTL waves make wave superposition possible in the following way, based on consideration of the Froude number. At the generation time, $F_i < 1$ for individual fast MTL waves and $F_i > 1$ for individual slow MTL waves propagating upstream. As the basic flow speeds up (slows down), the F_i values for the fast (slow) MTL wave components before (after) the maximum flow increase (decrease) toward unity. Thus, a superposition of fast (slow) MTL wave components generated in the acceleration (deceleration) stage before (after) the maximum flow in effect takes place.

It seems useful to seek the values of kU_0/σ_f, for which the propagation of MTL waves becomes similar to that of internal tides or unsteady lee waves. A situation similar to internal tides could be created by a condition under which slow (fast) MTL waves always move in the downstream (upstream) direction at their generation times. This condition requires that the signs of the absolute phase velocities $[c_{px}^{\pm}(t_0) + U(t)]$ are always same as those of the intrinsic phase velocities $[c_{px}^{\pm}(t_0)]$. It is then straightforward to derive that this is satisfied when $kU_0/\sigma_f < \frac{1}{2}$ $(kU_0/\sigma_f < 1)$ for the slow (fast) MTL waves, as confirmed by Figs. 2c and 2d. For a situation similar to unsteady lee waves, the propagation process shown below is probably best regarded as being similar to that of unsteady lee waves. Around the maximum flow, both slow and fast MTL wave components with maximum amplitude form wave fronts, which subsequently move in the upstream direction after the basic flow decelerates to speeds comparable to the wave speed (Figs. 2a,b). Such a situation occurs if both fast and slow MTL waves generated by the maximum flow reach their greatest phase speed. This condition always holds for fast MTL waves. For the slow MTL waves, the condition is realized when $kU_0/\sigma_f > 2$.

It is noteworthy that slow MTL wave components generated around the maximum flow have very small phase speeds (almost zero when $kU_0/\sigma_f = 1$) and large amplitudes, indicating that these components stay around the generation region for a relatively long time and simply move back and forth under the influence of advection. This implies that these MTL waves can be superposed and amplified over many periods and thereby can affect the mean state considerably. Since the behavior of such waves may depend on the approximation used in the relation between fixed and moving frames, particularly when $kU(t)/\sigma_f = 1$, a more detailed analysis may be required to clarify this effect.

The above features of MTL waves enable us to understand the reason why the short wave at the sill break in the M_2 case of NA is amplified, since kU_0/σ_f is 2.5, indicating that this wave is in the MTL wave regime. Moreover, our theoretical result also enables us to explain one unexplained numerical result of Lott and Teitelbaum (1993b). For the case $\varepsilon = 4.8$ in their study, which roughly corresponds to $kU_0/\sigma_f \sim 4$, waves are

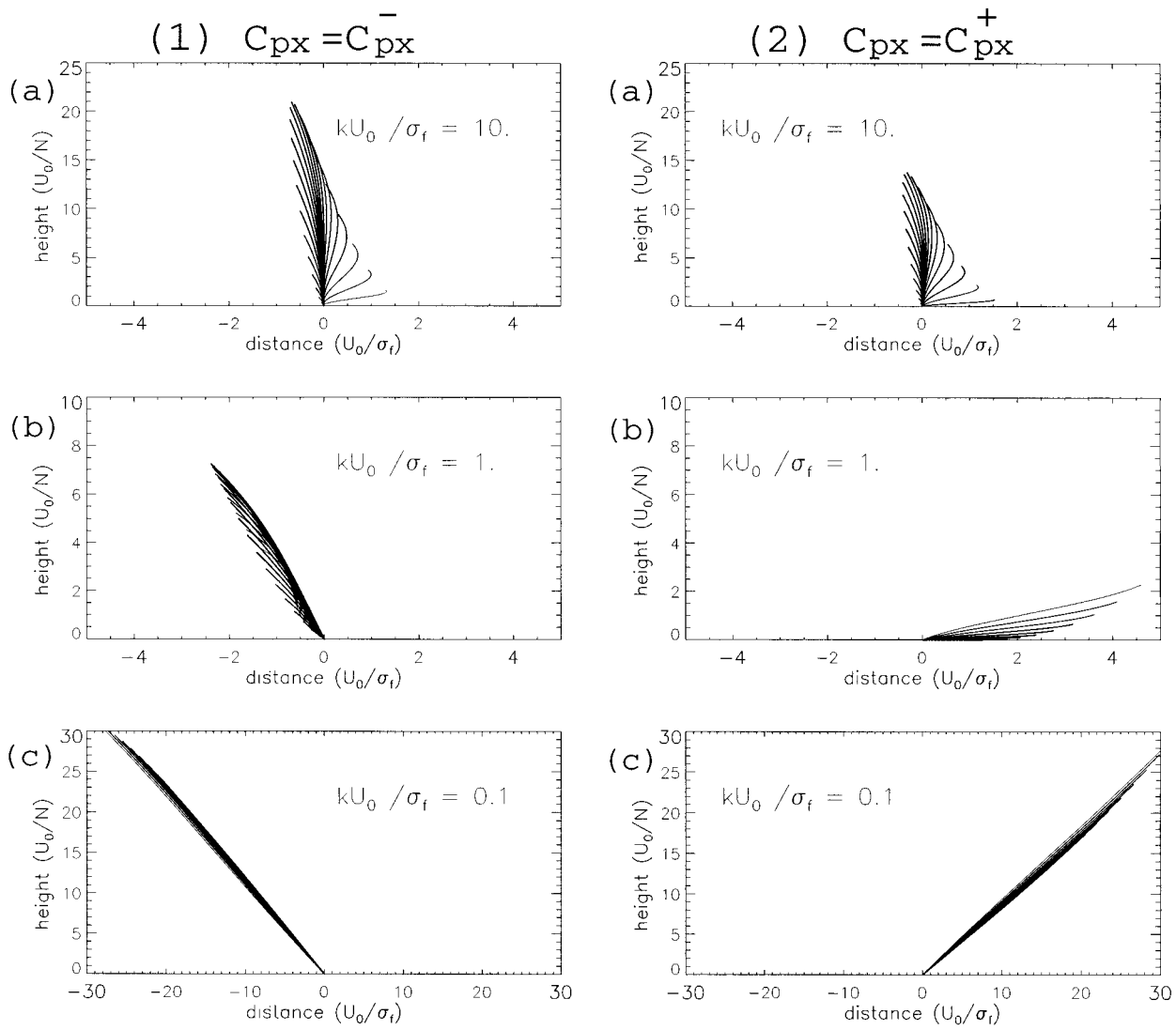

FIG. 3. Ray paths of individual wave components in $x - z$ space for a half tidal cycle, when the parameter kU_0/σ_f is 10 (a), 1 (b), and 0.1 (c).

also present on the upstream side at the maximum flow time. This cannot be explained by unsteady lee waves but can be explained on the basis of MTL waves, because individual fast MTL waves are faster than the basic flow at the generation time. An asymmetric wave pattern shown in the case of $\varepsilon = 0.4$ (i.e., $kU_0/\sigma_f \sim 0.5$) can also be explained by the difference in phase speeds between individual fast and slow MTL waves, and especially by our result that the phase speeds of the latter decrease with increase in the basic flow speed.

b. Propagation in the vertical direction

Next, we investigate propagation in the z direction. The vertical positions of wave components $z^{\pm}$ at time t under consideration are

$$z^{\pm}(t) = c_{gz}^{\pm}(t_0)(t - t_0) \simeq |c_{pz}^{\pm}(t_0)|(t - t_0). \qquad (6)$$

Using the same approximations for Eq. (1), the phase speed $c_{pz}^{\pm}$ can be written in terms of horizontal phase speeds as

$$|c_{pz}^{\pm}(t_0)| \simeq \frac{k}{N}(c_{px}^{\pm}(t_0))^2 \simeq \frac{k}{N}\left(U_0 \mp \frac{\sigma_f}{k}\right)^2, \qquad (7)$$

and hence the propagation in z–t space shows basically the same tendency as that in x–t space, when advection is absent.

Figure 3 summarizes the features of topographic internal wave propagation in terms of ray paths in x–z space for a half period. Unsteady lee wave components are highly dispersed around the locus of the wave component generated by the maximum flow, forming paths into a leaflike shape (Fig. 3a). They then continue to disperse and propagate upward at an oblique angle to

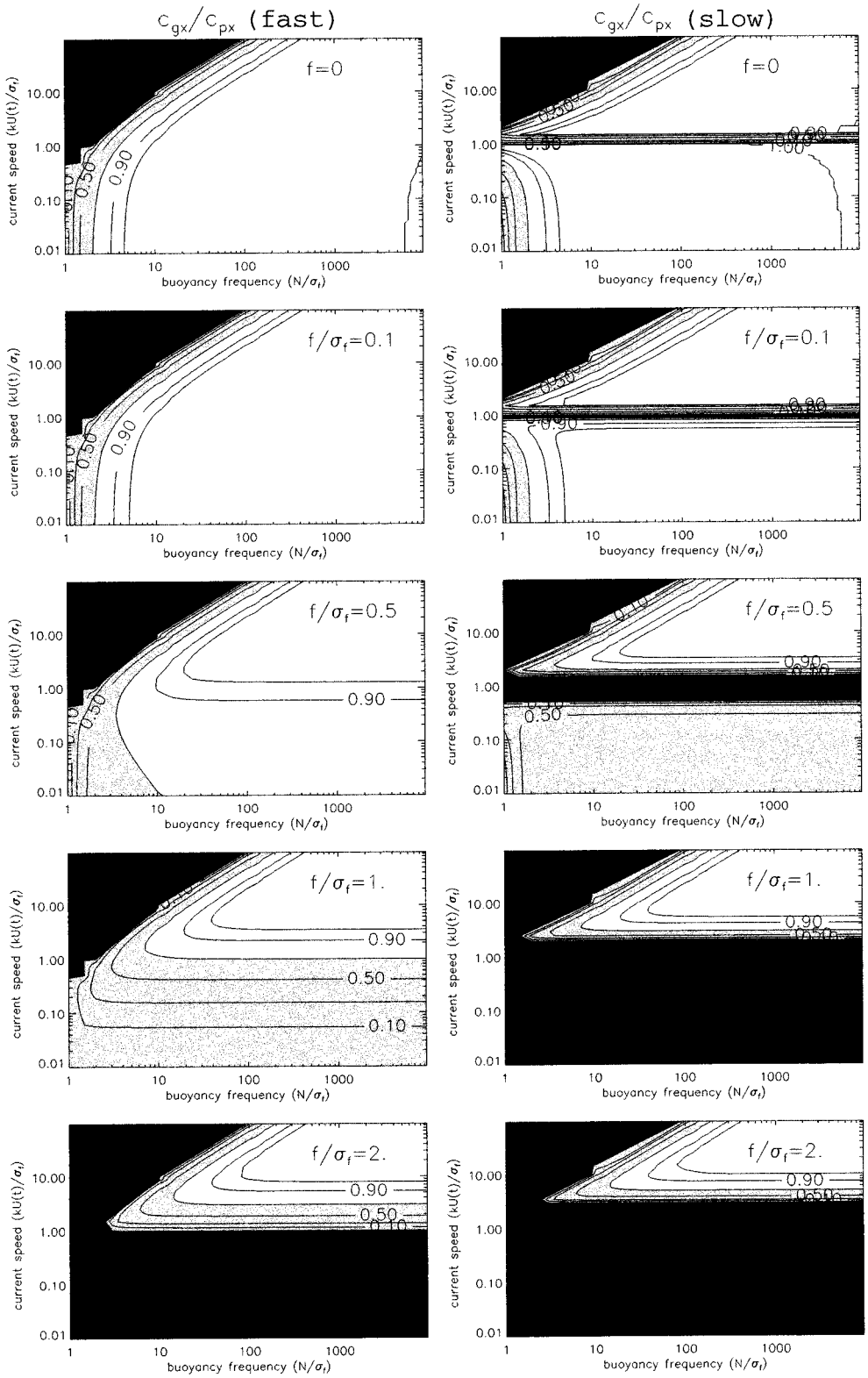

FIG. 4. The ratio of horizontal group velocity to phase velocities as a function of N/σ_f and kU/σ_f, when f/σ_f is 0, 0.1, 0.5, 1, and 2. Left- and right-hand columns correspond to fast and slow mixed tidal lee waves, respectively. Black regions indicate that wave components are not freely-propagating waves (subinertial), and shaded regions indicate that the ratio is less than 0.8.

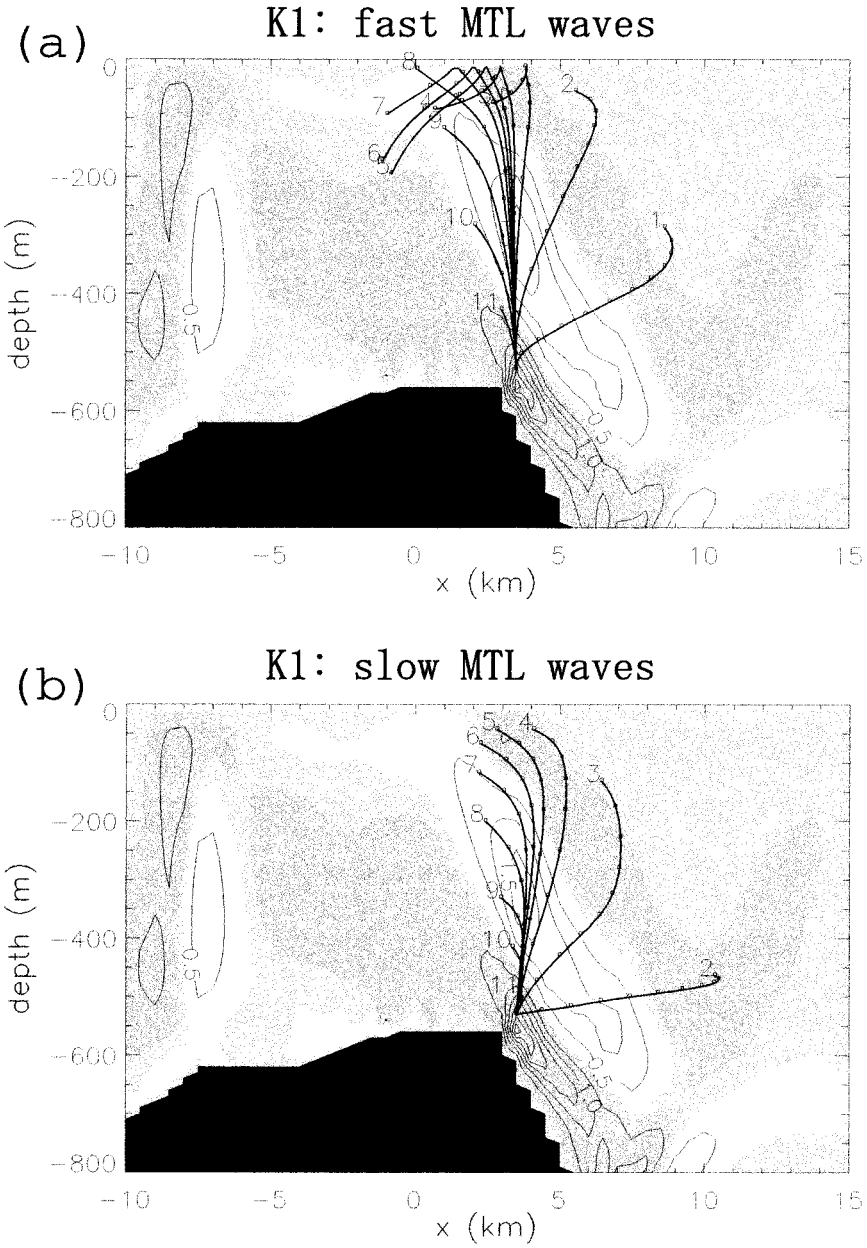

FIG. 5. The ray paths of (a) fast and (b) slow waves generated at the right-hand sill break in the K_1 case until half period. Calculations are performed using the numerical model results. The numbers indicate the time (hour) when the individual wave packets are launched. The superposed is the distribution of vertical velocity after half period. The contour interval is 0.5 cm s^{-1}. Values in nonshaded areas and the thicker shaded areas are positive and negative, respectively.

the vertical. This is basically the same as the result of Lott and Teitelbaum (1993b). In contrast, internal tide components are distributed in the well known V shape, with relatively little dispersion (Fig. 3c). When $kU_0/\sigma_f \sim 1$, both ray paths of fast and slow MTL wave components also form leaf shapes, and adding the two forms gives an asymmetrical V shape (Fig. 3b). Such a transition from internal tides to unsteady lee waves enhances the concentration of wave energy near the generation point. These features are also supported by the results of additional numerical experiments using cosine-shape isolated sills with various scales (not shown).

Superposition of wave components generated in the same half period occurs most effectively in the horizontal direction for the unsteady lee wave case and in the vertical direction for the MTL wave case. When

downward reflection at the sea surface occurs, superposition in the vertical direction could readily take place, thus enhancing the growth of these waves.

c. *Influence of the difference between phase velocity and group velocity*

As is clear from Eq. (1), the group speed is smaller than the phase speed in all wave regimes. The difference depends on the ratios of wave frequency to buoyancy frequency σ_i/N and wave frequency to the inertial frequency σ_i/f. Figure 4 shows the ratio of horizontal group speed to phase speed as a function of kU/σ_f and N for various f.

In the unsteady lee wave regime, the ratio c_{gx}/c_{px} decreases with increasing kU/N (i.e., with increasing frequency or decreasing stratification). This is marked in the very high frequency region, and hence waves for that region are effectively advected leeward since the basic flow speed is large and the group speed is significantly smaller than the phase speed, with the latter equal to the basic flow speed, as past studies have shown. The lower panels show that the decrease in the ratio c_{gx}/c_{px} with increasing f/σ_f is significant for waves close to internal tides. These waves are finally trapped at the topography when the basic flow is subinertial. Slow MTL waves are also effectively trapped when $kU(t)/\sigma_f \simeq 1$ since their frequencies become very small in this range. Note that unsteady lee waves and fast MTL waves can propagate freely even when the flow is subinertial, although the rotation effect is not negligible. In addition, the reduction in group speed of fast MTL waves caused by rotation may lead to enhanced superposition of their individual wave components in the generation region since the wave speeds decrease toward the basic flow speed.

A series of our experiments suggests that the assumption of $|c_{gx}| \simeq |c_{px}|$ is most valid when the ratio c_{gx}/c_{px} is greater than around 0.9. Otherwise the effect of the difference between the group and phase speeds should be added to the superposition processes of individual wave components discussed so far.

The ratios ($\sigma_{\max}/N$, $\sigma_{\max}/f$, c_{gx}/c_{px}) are (0.08, 0.31, 0.90) of the values presented in NA for the M_2 case, and (0.10, 0.24, 0.94) and (0.07, 0.34, 0.89) of the NA values for the fast and slow MTL waves, respectively, for the K_1 case. Hence, the approximation used in the previous sections will, in general, be valid, except for slow MTL waves in the present M_2 case, which are subinertial (here the maximum intrinsic frequency, $-kU_0 + \sigma_f$, is 0.7×10^{-4} s^{-1}). In this case the waves are trapped by the sill.

3. Ray tracing in the calculated field of NA

To demonstrate the effectiveness of our new amplification mechanism, we perform ray tracing of wave components evolving to large-amplitude compound waves in the K_1 and M_2 cases (see appendix B for the method). The basic states are determined from the calculated velocity and density fields of NA in order to take account of the effect of both spatial variations in flow and stratification on wave propagation. In particular, the strong stratification near the surface and the significant basic flow variation due to the presence of the large-amplitude sill are expected to influence the wave propagation considerably.

The ray paths traced up to 1/2 period for the K_1 and M_2 cases are shown in Figs. 5 and 6a, respectively. These figures show that the paths of MTL waves and unsteady lee waves eventually form leaf-shaped distributions with well-defined leading edges. The ray paths correspond to the positions of the wave packets (i.e., the center of wave energy), which agree well with the locations of strong vertical velocity for both cases. After 1/2 period, wave energy in the surface layer is much larger than in lower layers due to stronger stratification there. Accordingly, using ray tracing techniques, we can successfully explain the trapping and amplification of topographic internal waves in the K_1 and M_2 cases, a process that is difficult to explain using previous theories. Thus, our theoretical model is considered to be effective in describing wave growth processes within the limits of nonlinearity, duration, and the general applicability of the WKB approximation inherent in these cases.

For comparison, Figs. 6b and 6c show ray tracing results for initial wave frequencies set to those of the lee-wave (b) and internal-tide (c) constituents for the M_2 case. Clearly, the MTL wave case shown in Fig. 6a can best explain the position of the wave observed over the right-hand break in the model result. This also indicates the importance of the concept of MTL waves.

It should be noted that, when the amplitude of the bottom topography is finite, flow separation often takes place, so the particle flow paths are not strictly guided by the bottom topography. This corresponds to the present K_1 and M_2 cases for which the horizontal wavenumber of the generated waves cannot be simply determined from the curvature of the topography. In fact, the main streamline may be controlled by various parameters. For example, the shape of topography, the background flow speed, the buoyancy frequency, and the Coriolis parameter can play a role. Our understanding of the factors determining the relationship between the shape of the main streamline and such basic parameters remains partial so that here we have determined the horizontal wavelength from the calculated vertical-velocity distribution for convenience. Though our estimate shows that the horizontal scale derived from the curvature of the sill break topography ($\sim$5 km) is roughly comparable to that of the waves modeled here, the best means of determining horizontal wavelength still remains to be clarified. Nevertheless, the fact that a rough agreement between wave and sill scales exists suggests that the theoretical considerations made above

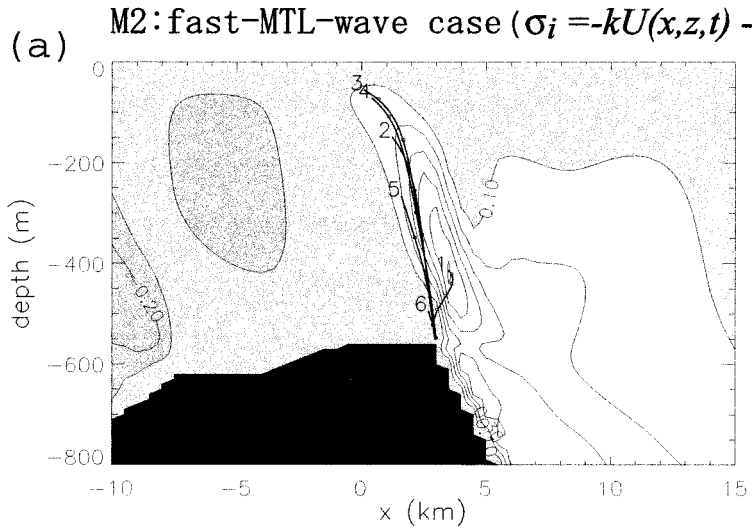

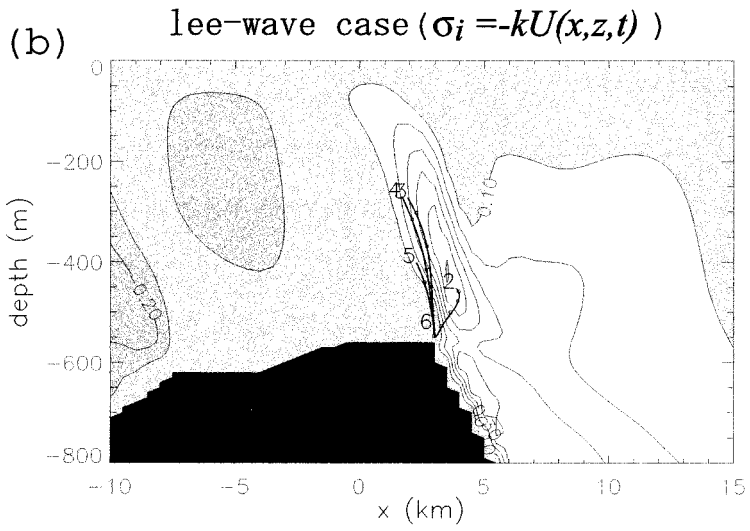

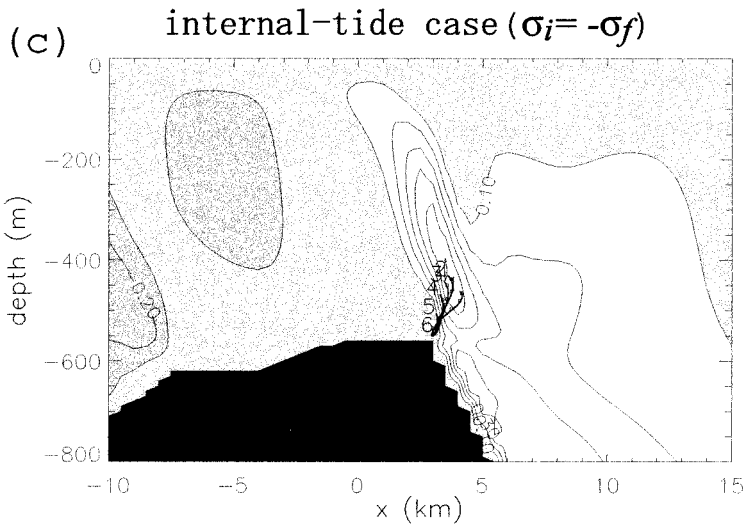

FIG. 6. As in Fig. 5 but for (a) the ray paths of fast MTL waves in the M_2 case. The results of additional experiments where initial *frequencies are set* to those of (b) lee waves and (c) internal tides are also shown. Contour interval of the vertical velocity after half period is 0.1 cm s^{-1}.

TABLE 3. Horizontal group velocities of topographic internal waves.

Wave regime		$\frac{kU_0}{\sigma_f} \gg 1$	$\frac{kU_0}{\sigma_f} \sim 1$	$\frac{kU_0}{\sigma_f} \ll 1$
parameter range		unsteady lee waves	mixed tidal–lee waves	internal tides
$f = 0$	$\sigma_i/N \sim 1$	$\frac{N^2 - (kU)^2}{U(k^2 + m^2)}$	$\frac{k[N^2 - (kU \pm \sigma_f)^2]}{(kU \pm \sigma_f)(k^2 + m^2)}$	$\frac{k[N^2 - \sigma_f^2]}{\sigma_f (k^2 + m^2)}$
	$\sigma_i/N \ll 1$	$-U(t)$	$-U(t) \pm \sigma_f/k$	$\pm\sigma_f/k$
$f < \sigma_f$		Almost the same as above		$\times(1 - f^2/\sigma_f^2)$
$f \geq \sigma_f$		$\times(1 - f^2/\sigma_i^2)$		Topographically trapped waves

on the basis of a linear approximation may help us to understand the basic features of the wave growth in the present numerical experiments.

The finite sill height also affects lee wave responses by producing variations in the basic flow as follows 1) A basic flow increases with decreasing depth so that wave trapping occurs more effectively on the downstream side (i.e., for waves propagating toward shallower water), as seen in Fig. 7 of NA. This fact can be easily confirmed by ray tracing with a spatially varying basic flow (not shown); 2) the generation regions of internal tides, which may work as a basic current for lee waves, are spatially broad; and 3) an overflow induces an intensified bottom current, which may enhance the generation of unsteady lee waves.

4. Summary and discussion

Table 3 shows an overview of the amplification mechanism discussed so far in terms of the intrinsic horizontal group speeds of topographic internal waves for each regime.

Unsteady lee waves, which are always amplified, grow most effectively in all three wave types when the maximum frequency is sufficiently small relative to the buoyancy frequency. Fast MTL waves are also effectively amplified as unsteady lee waves, when the reduction of the group speed due to rotation is so significant as appeared in the M_2 case. Thus, when the condition

$$\sigma_f \ll kU_0 \ll N \quad \text{or} \quad f \sim \sigma_f < kU_0 \ll N \qquad (8)$$

is satisfied, individual wave components generated around the maximum flow time are effectively trapped and superposed. Therefore, the topographic internal waves readily reach large amplitudes if the duration and/or magnitude of the forcing are sufficiently large. These effects can be estimated by $[(NU_0/\sigma_f)h_x]^2$, which indicates the increase of potential energy associated with the vertical excursion of isopycnal surfaces caused by the basic tidal flow (e.g., Baines 1982).

It should be noted that such trapping and amplification can occur even if the critical Froude number or the critical slope conditions required by previous theories are not satisfied. The reason for this is that these earlier conditions for wave growth cover only a part of the parameter range of topographic internal waves. For the critical slope theory, the corresponding range is $kU_0/\sigma_f \ll 1$ so that the generated waves are all identical to internal tides, and advection effects in both generation and amplification are neglected. The HI model assumed that 1) only internal tides are generated, 2) these waves form modal waves immediately after the generation, and 3) the group speed is almost equal to the eigenvalue of the corresponding mode and hence the phase speed (though implicitly). Thus, the HI model corresponds to the range of $kU_0/\sigma_f \ll 1$, $f^2 \ll \sigma_f^2$, and $\sigma_i^2 \ll N^2$. Accordingly, it is appropriate for long internal tides at low latitudes and/or when the typical horizontal scales are at most the internal radius of deformation. Also, if the HI model is extended to incorporate the effect of the change in frequency, it could be useful to describe the situation of almost flat bottom topography in shallow water where waves form modal structures immediately after the excitation.

Many observations show the generation of high-frequency waves over topography by an oscillatory flow, particularly in the context of continental shelfbreak features (e.g., Chereskin 1983; Sandstrom and Elliott 1984; Holloway 1985, 1987; Park 1986; Loder et al. 1992; New and Pingree 1992; Liu et al. 1998). Some of the waves could be excited as unsteady lee and/or MTL waves, which may be amplified by the mechanism discussed above. For example, Holt and Thorpe (1997) suggested that around 25% of the high-frequency internal wave packets observed in the Celtic Sea have orientations consistent with generation by an alongslope flow over rough topography on the slope. Considering the dominance of tidal currents there and the smallness of the horizontal scale of the topography, these packets are expected to be excited as unsteady lee waves. Another example is the observation by Kuroda and Mitsudera (1995) in the East China Sea, which was mentioned in the introduction. The growth of the observed waves could be explained on the basis of the new concepts introduced in this paper, though Kuroda and Mitsudera (1995) considered the growth to result from nonlinearities due to finite wave amplitudes.

Care should be taken, however, when identifying unsteady lee waves with observations at a fixed point, such

as a mooring, since discrimination of unsteady lee waves from internal tides is difficult around the generation region because the former are trapped until the flow direction changes. This can be easily understood by considering the Doppler relation. The intrinsic frequencies of topographic internal waves generated at $x = x_0$ and $t = t_0$ are $-kU(x_0, t_0) \pm \sigma_f$, but the frequencies at a fixed point x are observed as $+kU(x, t) - kU(x_0, t_0) \pm \sigma_f$.

In this study, we have revealed the topographic internal wave growth by focusing only on the relation to the important parameter, kU_0/σ_f. In doing so, because ray tracing strictly applies only when the waves are in slowly varying ambient conditions, our investigation is rather qualitative. Also, some physical factors are missing in our model. We have neglected the nonlinear effects caused by large wave amplitudes, though this might be acceptable because our primary interest is in how topographic internal waves are amplified to such large amplitudes. However, after the waves have grown sufficiently, we should incorporate nonlinear wave effects such as breaking of lee waves at the generation region. In addition, wave generation becomes more complicated in three dimensions due to the more complex flow and the changes in buoyancy frequency that develop around obstacles. Background flows, such as wind-driven and thermohaline circulations, modify the basic flow and thus may affect the generation and evolution of the waves. These problems are left for future work.

Acknowledgments. We wish to acknowledge Prof. J. P. Matthews at Kyoto University for his critical reading. We also thank anonymous reviewers for their invaluable comments. Numerical calculations were done on the FACOM M1800 and VP2600 at the Data Processing Center of Kyoto University.

APPENDIX A

Method for Estimating the Contribution Rate and Relative Magnitude

In this study, the ''contribution rate'' of the mth mode ($m = 1, 2, \cdots$) is defined, for convenience, as

$$\left(W_m^2 \int N^2 R_m^2 \, dz\right) \Big/ \left(\int N^2 w^2 \, dz\right) \times 100(\%),$$

where R_m and W_m are the eigenfunction and its coefficient for the mth mode (i.e., $w = \Sigma_m W_m R_m$). Theoretically, the sum of the contribution rates for all m should be exactly 100%, so the excess from this value gives the error magnitude (here approximately 2%) in calculating the decomposition. Also, the ''relative magnitude'' of the mth mode is defined here as the value of the coefficient corresponding to the eigenfunction when normalized to a maximum value of unity.

APPENDIX B

Method of Ray Tracing in the Calculated Field of NA

If we neglect the effect of currents induced by waves themselves, the propagation of wave packets in a gradually varying basic state can be described by the following equations (Lighthill 1978):

$$\frac{dx_i}{dt} = U_i + \frac{\partial \sigma}{\partial k_i}, \tag{B1}$$

$$\frac{dk_i}{dt} = -k_j \frac{\partial U_j}{\partial x_i} - \frac{\partial \sigma}{\partial x_i}, \tag{B2}$$

where $U_i (U_{1,2} = U, W)$ and $k_i (k_{1,2} = k, m)$ denote the basic flow speed and wavenumber in the $x_i (x_{1,2} = x, z)$ direction, respectively, and d/dt is the temporal change along the ray. Equation (B1) gives the velocity of a wave packet along its ray path, which consists of the basic flow vector responsible for advecting the packet and the group velocity of the wave. Equation (B2) describes the refraction of a wave packet due to the spatially varying basic flow and stratification. To complete the set of equations we use the linear dispersion relation,

$$\sigma^2 = (N^2K^2 + f^2m^2)(k^2 + m^2)^{-1}. \tag{B3}$$

The ray tracing equations then become

$$\frac{dx}{dt} = U + \frac{k}{\sigma} \frac{N^2 - \sigma^2}{m^2 + k^2}, \tag{B4}$$

$$\frac{dz}{dt} = W - \frac{m}{\sigma} \frac{\sigma^2 - f^2}{m^2 + k^2}, \tag{B5}$$

$$\frac{dk}{dt} = -\left(k \frac{\partial U}{\partial x} + m \frac{\partial W}{\partial x}\right) - \frac{1}{2\sigma} \frac{k^2}{m^2 + k^2} \frac{\partial N^2}{\partial x}, \tag{B6}$$

$$\frac{dm}{dt} = -\left(k \frac{\partial U}{\partial z} + m \frac{\partial W}{\partial z}\right) - \frac{1}{2\sigma} \frac{k^2}{m^2 + k^2} \frac{\partial N^2}{\partial z}. \tag{B7}$$

Here we set $W = 0$ in order to avoid the influence of currents induced by the traced wave itself. Numerical integration of these ordinary differential equations with a fourth-order Runge–Kutta method enables us to trace individual wave components generated at various times. For the initial wave structure, we determine the horizontal wavelength as 8 km and 6 km for the K_1 and M_2 case, respectively, from the vertical velocity distribution. The wave frequency is taken as $-kU(t) \pm \sigma_f$, and we require the vertical wavenumber to satisfy the dispersion relation. Then, the effect of temporal variations in the basic state is incorporated through the basic state variables (U, N) and the initial wave frequency. The initial position of wave packets is set to be the right-hand sill break where the large-amplitude waves are generated. When wave packets reach the surface, they are perfectly reflected.

REFERENCES

Baines, P. G., 1982: On internal tide generation models. *Deep-Sea Res.,* **29,** 307–338.

Bannon, P. R., and J. A. Zehnder, 1985: Surface pressure and mountain drag for transient airflow over a mountain ridge. *J. Atmos. Sci.,* **42,** 2454–2462.

Bell, T. H., 1975: Lee waves in stratified flows with simple harmonic time dependence. *J. Fluid Mech.,* **67,** 705–722.

Chereskin, T. K., 1983: Generation of internal waves in Massachusetts Bay. *J. Geophys. Res.,* **88,** 2649–2661.

Craig, P. D., 1987: Solutions for internal tidal generation over coastal topography. *J. Mar. Res.,* **45,** 83–105.

Farmer, D. M., and J. D. Smith, 1980: Tidal interaction of stratified flow with a sill in Knight Inlet. *Deep-Sea Res.,* **27,** 239–254.

Gerkema, T., and J. T. F. Zimmerman, 1995: Generation of nonlinear internal tides and solitary waves. *J. Phys. Oceanogr.,* **25,** 1081–1094.

Grimshaw, R. H., and N. Smyth, 1986: Resonant flow of a stratified fluid over topography. *J. Fluid Mech.,* **169,** 429–464.

Hibiya, T., 1986: Generation mechanism of internal waves by tidal flow over a sill. *J. Geophys. Res.,* **91,** 7696–7708.

Holloway, P. E., 1985: A comparison of semidiurnal internal tides from different bathymetric locations on the Australian North West Shelf. *J. Phys. Oceanogr.,* **15,** 240–251.

——, 1987: Internal hydraulic jumps and solitons at a shelf break region on the Australian North West Shelf. *J. Geophys. Res.,* **92,** 5405–5416.

Holt, J. T., and S. A. Thorpe, 1997: The propagation of high frequency internal waves in the Celtic Sea. *Deep-Sea Res.,* **44,** 2087–2116.

Huthnance, J. M., 1989: Internal tides and waves near the continental shelf edge. *Geophys. Astrophys. Fluid Dyn.,* **48,** 81–106.

Kono, T., and Y. Kawasaki, 1997: Modification of the western subarctic water by water exchange with the Okhotsk Sea. *Deep-Sea Res.,* **44,** 689–711.

Kuroda, Y., and H. Mitsudera, 1995: Observation of internal tides in the East China Sea with an underwater sliding vehicle. *J. Geophys. Res.,* **100,** 10 801–10 816.

Lee, C.-Y., and R. C. Beardsley, 1974: The generation of long nonlinear internal waves in a weakly stratified shear flow. *J. Geophys. Res.,* **79,** 453–462.

Lighthill, M. J., 1978: *Waves in Fluids.* Cambridge University Press, 504 pp.

Liu, A. K., J. R. Holbrook, and J. R. Apel, 1985: Nonlinear internal wave evolution in the Sulu Sea. *J. Phys. Oceanogr.,* **15,** 1613–1624.

——, Y. S. Chang, M.-K. Hsu, and N. K. Liang, 1998: Evolution of nonlinear internal waves in the East and South China Seas. *J. Geophys. Res.,* **103,** 7995–8008.

Loder, J. W., D. Brickman, and E. P. W. Horne, 1992: Detailed structure of currents and hydrography on the northern side of Georges Bank. *J. Geophys. Res.,* **97,** 14 331–14 351.

Lott, F., and H. Teitelbaum, 1993a: Topographic waves generated by a transient wind. *J. Atmos. Sci.,* **50,** 2607–2624.

——, 1993b: Linear unsteady mountain waves. *Tellus,* **45A,** 201–220.

Lukas, R., T. Yamagata, and J. P. McCreary, 1996: Pacific low-latitude western boundary currents and the Indonesian Throughflow. *J. Geophys. Res.,* **101,** 12 209–12 216.

Mazé, R., 1987: Generation and propagation of non-linear internal waves induced by the tide over a continental slope. *Contin. Shelf Res.,* **7,** 1079–1104.

Nakamura, T., T. Awaji, T. Hatayama, K. Akitomo, T. Takizawa, T. Kono, and M. Fukasawa, 2000: The generation of large-amplitude unsteady lee waves by subinertial K_1 tidal flow: A possible vertical mixing mechanism in the Kuril Straits. *J. Phys. Oceanogr.,* **30,** 1601–1621.

New, A. L., and R. D. Pingree, 1992: Local generation of internal soliton packets in the central Bay of Biscay. *Deep-Sea Res.,* **39,** 1521–1534.

Park, Y.-H., 1986: Semidiurnal internal tides on the continental shelf off Abidjan. *J. Phys. Oceanogr.,* **16,** 1585–1592.

Rattray, M., J. G. Dworski, and P. E. Kovala, 1969: Generation of long internal waves at the continental slope. *Deep-Sea Res.,* **16,** s179–s195.

Sandstrom, H., and J. A. Elliott, 1984: Internal tide and solitons on the Scotian Shelf: A nutrient pump at work. *J. Geophys. Res.,* **89,** 6415–6426.

Sherwin, T. J., 1988: Analysis of an internal tide observed on the Malin shelf, north of Ireland. *J. Phys. Oceanogr.,* **18,** 1035–1050.

——, and N. Taylor, 1990: Numerical investigations of linear internal tidal generation in the Rockall Trough. *Deep-Sea Res.,* **37,** 1595–1618.

Smyth, N. F., and P. E. Holloway, 1988: Hydraulic jump and undular bore formation on a shelf break. *J. Phys. Oceanogr.,* **18,** 947–962.

Talley, L. D., 1991: An Okhotsk Sea water anomaly: Implications for ventilation in the North Pacific. *Deep-Sea Res.,* **38,** s171–s190.

Thorpe, S. A., 1992: The generation of internal waves over the rough topography of the continental slope. *Proc. Roy. Soc. London,* **439A,** 115–130.

——, 1996: The cross-slope transport of momentum by internal waves generated by along-slope currents over topography. *J. Phys. Oceanogr.,* **26,** 191–264.

Willmott, A. J., and P. D. Edwards, 1987: A numerical model for the generation of tidally forced nonlinear internal waves over topography. *Contin. Shelf Res.,* **7,** 457–484.

Wunsch, C., 1969: Progressive internal waves on slopes. *J. Fluid Mech.,* **35,** 131–144.

——, 1975: Internal tides in the ocean. *Rev. Geophys. Space Phys.,* **13,** 167–182.